DIRECT ACCELERATION OF PICKUP IONS
AT THE SOLAR WIND TERMINATION SHOCK:
THE PRODUCTION OF ANOMALOUS COSMIC RAYS

Donald C. Ellison
Department of Physics
North Carolina State University
Raleigh, NC 27695, U.S.A.

Frank C. Jones and Matthew G. Baring
Laboratory for High Energy Astrophysics
NASA Goddard Space Flight Center
Greenbelt, MD 20771, U.S.A.

DIRECT ACCELERATION OF PICKUP IONS AT THE SOLAR WIND TERMINATION SHOCK: THE PRODUCTION OF ANOMALOUS COSMIC RAYS

DONALD C. ELLISON
Department of Physics, North Carolina State University,
Box 8202, Raleigh NC 27695, U.S.A.
don_ellison@ncsu.edu

FRANK C. JONES & MATTHEW G. BARING[1]
Laboratory for High Energy Astrophysics,
NASA Goddard Space Flight Center, Greenbelt, MD 20771, U.S.A.
frank.c.jones@gsfc.nasa.gov, baring@lheavx.gsfc.nasa.gov
The Astrophysical Journal, in press

ABSTRACT

We have modeled the injection and acceleration of pickup ions at the solar wind termination shock and investigated the parameters needed to produce the observed Anomalous Cosmic Ray (ACR) fluxes. A non-linear Monte Carlo technique was employed, which in effect solves the Boltzmann equation and is not restricted to near-isotropic particle distribution functions. This technique models the injection of thermal and pickup ions, the acceleration of these ions, and the determination of the shock structure under the influence of the accelerated ions. The essential effects of injection are treated in a mostly self-consistent manner, including effects from shock obliquity, cross-field diffusion, and pitch-angle scattering. Using recent determinations of pickup ion densities, we are able to match the absolute flux of hydrogen in the ACRs by assuming that pickup ion scattering mean free paths, at the termination shock, are much less than an AU and that modestly strong cross-field diffusion occurs. Simultaneously, we match the flux *ratios* He^+/H^+ or O^+/H^+ to within a factor ~ 5. If the conditions of strong scattering apply, *no pre-termination-shock injection phase is required* and the injection and acceleration of pickup ions at the termination shock is totally analogous to the injection and acceleration of ions at highly oblique interplanetary shocks recently observed by the Ulysses spacecraft. The fact that ACR fluxes can be modeled with standard shock assumptions suggests that the much-discussed "injection problem" for highly oblique shocks stems from incomplete (either mathematical or computer) modeling of these shocks rather than from any actual difficulty shocks may have in injecting and accelerating thermal or quasi-thermal particles.

Subject headings: Cosmic rays: general — particle acceleration — shock waves — diffusion — interplanetary medium — termination shock

1. INTRODUCTION

It is believed that Anomalous Cosmic Rays (ACRs) originate as interstellar pickup ions (Fisk, Kozlovsky, & Ramaty 1974) which are accelerated at the solar wind termination shock (Pesses, Jokipii, & Eichler 1981). Such ions originate as neutrals that are swept into the solar system from the external interstellar medium, and subsequently ionized by the solar UV flux or by charge exchange with solar wind ions. Recent observations of pickup ions by the Ulysses spacecraft (e.g. Gloeckler et al. 1993) adds to the indirect evidence for this scenario, which by now has become quite compelling. However, one essential element of the process, namely how pickup ions are first injected into the acceleration mechanism, has engendered controversy. We show here that standard and well-tested assumptions of diffusive (also called first-order Fermi) shock acceleration allow the direct injection and acceleration of pickup ions without a pre-injection stage. We have employed our Monte Carlo simulation code (e.g. Ellison, Baring, & Jones 1996) to study the physical parameters that the solar wind termination shock must have in order to produce the observed ACR fluxes.

For input at the termination shock, we use a standard expression for the shape of the isotropic pickup ion phase-space distribution based on the derivation of Vasyliunas & Siscoe (1976) (e.g. Gloeckler et al. 1993, 1994; le Roux, Potgieter, & Ptuskin 1996), and normalize this to the values reported by Cummings & Stone (1996) for the interstellar ion flux in the heliosphere (see also Stone et al. 1996; Isenberg 1997). We use the Cummings & Stone fluxes, even though more recent values have been reported (e.g. Gloeckler 1996; Gloeckler, Fisk, & Geiss 1997), so we can make a direct comparison with their results. In addition, since important parameters are uncertain at the termination shock, we perform a limited parameter survey but always find that we can easily match the observed flux of H^+, by varying the strength of scattering. For typical cases, we require that $\lambda_\| \sim$ 5-10 r_g, where $\lambda_\|$ is the scattering mean free path parallel to the mean magnetic field and r_g is the ion gyroradius. This length scale of diffusion parallel to the field seems fairly typical of that inferred in the vicinity of planetary bow shocks (Ellison, Möbius, & Paschmann 1990), interplanetary shocks (Baring et al. 1997), supernova shocks (Achterberg, Blandford, & Reynolds 1994), and that found in hybrid simulations of quasi-parallel shocks (e.g. Giacalone, et al. 1993) but is

[1] Universities Space Research Association

much less than that found for the *undisturbed* interplanetary medium (e.g. Forman, Jokipii, & Owens 1974; Palmer 1982; Moussas et al. 1992; Bieber et al. 1994; Gloeckler, Fisk, & Geiss 1997). If the turbulence we postulate for pickup ions is, in fact, present, it implies that the termination shock generates fairly strong, local magnetic field turbulence as has long been observed or inferred at other collisionless shocks (e.g. Lee 1982; 1983 and references therein). We are somewhat less successful in matching the ACR flux *ratios*, He^+/H^+ and O^+/H^+, seeing less enhancement based on mass/charge than reported by Cummings & Stone (1996). We do, however, match the ratios to within a factor of $\sim$ 5, a relatively small difference given the uncertainties of extrapolating flux densities to the termination shock and the possibility that species-dependent heating or pre-acceleration could occur in the solar wind before pickup ions reach the termination shock.

Regardless of any uncertainty about flux ratios, that fact that we can model the *absolute* hydrogen flux with no pre-acceleration is in clear contradiction with the conclusions of most previous work addressing pickup ion injection at the termination shock. For the most part, previous work has argued that the highly oblique termination shock would not be able to accelerate pickup ions directly. It was postulated, for example, that some independent pre-acceleration phase, perhaps at interplanetary shocks (e.g. Jokipii & Giacalone 1996) or by second-order Fermi acceleration off Alfvén waves (e.g. Isenberg 1986; Bogdan, Lee, & Schneider 1991; Fichtner et al. 1996), or transit-time damping of magnetosonic waves (e.g. Fisk 1976; Schwadron, Fisk, & Gloeckler 1996), or shock 'surfing' (e.g. Lee et al. 1996; Zank et al. 1996) was necessary before the pickup ions encountered the termination shock and underwent their final acceleration to ACR energies. It has also been suggested that the termination shock was not quasi-perpendicular for a substantial fraction of the time (e.g. Liewer, Rath, & Goldstein 1995; Chalov & Fahr 1996b) thus allowing injection at times when the shock was less oblique. Furthermore, Chalov & Fahr (1996b) and Le Roux, Potgieter, & Ptuskin (1996) suggest that reflected pickup ions from an already energized population serve as seed particles for Fermi acceleration. While it is certainly possible that some pre-acceleration may occur or that the shock is highly variable, our results indicate that the termination shock seems fully capable of injecting and accelerating pickup ions directly in a single step if standard diffusive shock acceleration assumptions are made and if the self-generated turbulence is as strong as routinely assumed in virtually all other astrophysical shocks which accelerate particles. Since diffusive shock acceleration predictions have been tested extensively and successfully at directly observable shocks in the inner heliosphere (and less directly at shocks outside the heliosphere), we see no physical reason why the termination shock should act differently, i.e. should be incapable of generating sufficient turbulence, or why standard shock assumptions shouldn't apply (e.g. Drury 1983; Jones & Ellison 1991). We note that claims of extremely weak scattering of pickup ions ($\lambda_\parallel \sim$AU) seem to be based on modeling of the *quiet* interplanetary medium (Gloeckler, Fisk, & Geiss 1997; Fisk et al. 1997; Möbius et al. 1998). Convincing evidence that the mean free paths of pickup ions with energies much less than ACR energies are $\sim$ AU *immediately behind* an inter-

planetary shock would, of course, make the diffusive shock acceleration of these particles to ACR energies impossible, since some particles must be able to diffuse back to the shock from the downstream region in order to obtain MeV energies.

Our nonlinear shock acceleration model calculates the full distribution functions of the various ion species at the shock including effects from the shock smoothing produced by the back-reaction of accelerated particles on the solar wind flow. The three most abundant ACR species, H^+, He^+, and O^+, are included self-consistently in the determination of the shock structure. Since our Monte Carlo technique has not yet been generalized to spherical geometry, we are forced to assume that the termination shock is plane. However, the most important process we investigate, the injection of pickup ions, occurs locally and will not be seriously affected by this approximation. In addition, this implementation of the Monte Carlo simulation does not treat solar modulation in a complete fashion, nor does it include adiabatic losses; we anticipate including these in future work. For now, we artificially mimic the effects of adiabatic losses and truncate acceleration by placing a free escape boundary upstream from the plane shock. We also neglect the presence of galactic cosmic rays on the shock structure, relying on the estimate of Fisk (1996) that galactic cosmic rays will not produce pressure gradients strong enough to smooth the termination shock.

The most important model parameter we require is $\eta = \lambda_\parallel/r_g$, the ratio of the particle mean free path parallel to the magnetic field to the particle's gyroradius, and this is chosen to match observed spectral intensities. For a given η, our model gives the absolute normalization of all spectra at the shock. Unfortunately, the absolute intensities are strongly dependent on the pickup ion densities at the termination shock which are uncertain. Our determination of the *relative* intensities of different ion species, however, is not influenced in any important way by the absolute normalization or by small changes in η, although changes in Mach number can affect relative intensities as we show below. In partial support of the findings of Cummings & Stone (1996), we see evidence for an acceleration efficiency that increases with A/Q (mass number to charge number). The actual values that we obtain, however, are less than those inferred by Cummings & Stone. Similar A/Q enhancement effects have been reported for diffuse ions observed at the quasi-parallel Earth bow shock (Ellison, Möbius, & Paschmann 1990).

2. MODEL

The Monte Carlo technique we use here has been described in Ellison, Baring, & Jones (1996) and we refer the reader to that paper for complete details. Briefly, we have developed a technique for calculating the structure of a plane, steady-state, collisionless shock of arbitrary obliquity and arbitrary sonic and Alfvén Mach numbers greater than one. We include the injection and acceleration of ions directly from the background plasma and assume that, with the exception of pickup ions, no *ad hoc* population of superthermal seed particles is present. The model assumes that the background plasma, including accelerated particles, and magnetic fields are dynamically important and their effects are included in determining the shock structure. The most important difference between the code we

employ here and that described in Ellison, Baring, & Jones is that we are no longer restricted to subluminal shocks, i.e. shock geometries where the de Hoffmann-Teller (H-T) speed is less than the speed of light (note, however, that our application in this paper to the termination shock still focuses on subluminal shocks). We no longer move particles by transforming into the H-T frame, a frame where the $\mathbf{u} \times \mathbf{B}$ electric field disappears. Instead, we move particles in the normal incidence frame and explicitly include effects of the $\mathbf{u} \times \mathbf{B}$ field in translating the particles, allowing us to model shocks of arbitrary obliquity. Apart from this generalization, and the injection of pickup ions, the code used here is essentially identical to that described in Ellison, Baring, & Jones (1996).

The most basic assumption we make is that the complicated plasma physics can be described by a simple scattering relation for individual particles, i.e. ,

$$\lambda_{\parallel} = \eta r_g \quad \text{or} \quad \kappa_{\parallel} = \frac{1}{3} \eta r_g v \; , \qquad (1)$$

where v is the particle's speed in the local frame, $r_g = pc/(QeB)$ is the gyroradius of a particle of momentum p and charge Qe, $\lambda_{\parallel}$ is the mean free path parallel to the local magnetic field, $\kappa_{\parallel}$ is the diffusion coefficient parallel to the local magnetic field, and η is a model parameter which characterizes the strength of scattering and the importance of cross-field diffusion. We assume η is a constant independent of particle energy, particle species, and position relative to the shock. It's clear from equation (1), that as a particle convects, it will on average scatter after moving a distance $\lambda_{\parallel}$ along the magnetic field. We assume the particles pitch-angle scatter elastically and isotropically in the local plasma frame regardless of their energy. After each pitch-angle scattering (which occurs every $\delta t \ll \lambda_{\parallel}/v$) a new direction is obtained for a particle's velocity vector and a new gyrocenter is calculated. After some number of scatterings, a particle's pitch angle will deviate by $\sim 90°$ from it's original direction and it will be gyrating around a field line within $2r_g$ of the one the particle was circling originally. Such cross field diffusion is an integral part of diffusive acceleration at oblique shocks (e.g. Jokipii 1987; Ostrowski 1988) and Ellison, Baring, & Jones (1995) showed that the scheme we employ here and in Ellison, Baring, & Jones (1996) for cross-field diffusion, together with the assumption contained in equation (1), is equivalent to a kinetic theory description of diffusion (e.g. Axford 1965; Forman, Jokipii, & Owens 1974; Jones 1990), where the diffusion coefficients perpendicular to ($\kappa_{\perp}$) and parallel to ($\kappa_{\parallel}$) the mean field direction are related via $\kappa_{\perp} = \kappa_{\parallel}/(1 + \eta^2)$. The parameter η in equation (1) then clearly determines the "strength" of the scattering and when $\eta \sim 1$, $\kappa_{\perp} \sim \kappa_{\parallel}$ and particles diffuse across the magnetic field as quickly as they move along it (the so-called Bohm limit). The properties of highly oblique and quasi-parallel shocks tend to merge when the scattering is strong (i.e. $\eta \ll 10$).

We simplify our model of the termination shock in several important ways, namely we assume that the shock is plane and in a steady-state. While the steady-state assumption is sensible for the termination shock unless it is undergoing some form of perturbation on time scales short compared to the acceleration time of the ACRs, it is less

clear that a plane shock assumption is valid for the curved termination shock. However, the curvature of the termination shock will only be important if the diffusion length of particles is comparable to the shock radius, at which point high energy particles tend to leak away from the shock and the acceleration ceases. Otherwise the shock appears planar to the accelerating particles. Adiabatic losses in the expanding solar wind are more of a concern, since these losses can be shown to set the maximum energy particles obtain (Jones, in preparation). For our work here, we parameterize the maximum energy obtainable by placing a free escape boundary at a distance upstream from the shock. The distance is chosen to give maximum energies ~ 100 MeV, typical of ACRs. We find (we believe coincidentally) that the diffusion lengths of the highest energy particles *along the magnetic field* are comparable to the pole-to-equator distance. Since our models generally have $\kappa_{\perp} \ll \kappa_{\parallel}$, the maximum scalelength perpendicular to the termination shock (i.e. in the radial direction) is much shorter, of the order of a few AU.

Another important simplification is that we do not include a cross-shock, charge separation potential in our model. A cross-shock potential should exist and such a potential may have some effect on injection. We leave this generalization to later work.

Once a satisfactory model for oblique shocks and shock acceleration is developed, it becomes clear that the major problem with modeling a given source is the array of parameters that are required. Oblique shocks are complicated and we do not see how they can be modeled self-consistently without a large number of both environmental (e.g. Mach numbers, shock speed, size, obliquity, etc.) and model (e.g. η, type of scattering assumed, cross-shock potential, etc.) parameters. While simplifications and a reduction in the number of parameters can be made in some circumstances, the most extreme and useful being the assumption of a plane-parallel shock ($\Theta_{Bn} = 0$ everywhere, where Θ_{Bn} is the angle between the magnetic field and the shock normal), they cannot be made if the obliquity and particle acceleration are important, i.e. if the accelerated particles are numerous enough so that a test-particle solution is unrealistic. In this case, all of the parameters become important and must be included.

3. RESULTS

The upstream parameters required for a solution are: the shock speed, $V_{sk} = V_{sw}$ (in the solar wind frame), the magnetic field strength, B, the obliquity, Θ_{Bn}, the temperature, T, the number densities of the various thermal ion species, n_i, and the number densities of the various pickup ions, n_i^{pu}, all of which are ambient upstream conditions and can, in principle, be determined by observations (we assume that the termination shock is stationary so that the shock speed equals the solar wind speed, V_{sw}). Here, "upstream" means far enough in front of the shock so that backstreaming energetic particles do not influence the flow parameters. We also require our model parameter, η, and our scattering assumption, equation (1), which depend on the highly complex plasma interactions that occur in the shock environs. In principle, these could be determined by comparison with observations of space plasma shocks or 3-D plasma simulations; the prescription in equation (1) is

a simple and transparent way to model these plasma processes.

In addition to all of the above, we must also define the size of the acceleration region by setting the distance (in units of mean free paths), d_{FEB}, between the upstream free escape boundary (FEB) and the shock. Accelerated particles that diffuse upstream of the FEB are removed from the system, producing a high energy turnover in the spectrum and giving a crude approximation of adiabatic losses. We emphasize that this complexity and array of parameters is intrinsic to oblique shocks and must be included in any realistic model.

3.1. Parameters at the Termination Shock

We use a simple model to relate values for solar wind parameters at the termination shock to those at 1 AU. Assuming that the solar wind speed remains constant in its passage to the outer heliosphere, the density of a solar wind ion species at the termination shock is

$$n_{i,TS} = \left(\frac{1AU}{D_{TS}}\right)^2 n_{i,AU} , \qquad (2)$$

the magnetic field at the termination shock is

$$B_{TS} = \left(\frac{1AU}{D_{TS}}\right) B_{AU} , \qquad (3)$$

and the temperature of an ion species at the termination shock is

$$T_{i,\,TS} = \left(\frac{1AU}{D_{TS}}\right)^{2(\gamma_{sw}-1)} T_{i,\,AU} , \qquad (4)$$

where D_{TS} is the distance to the termination shock, the subscript "AU" indicates values at Earth, and the subscript "TS" indicates values at the termination shock. We have assumed that the solar wind flux per solid angle is conserved, and that the magnetic field strength decreases as r^{-1} in the tightly-wound Archimedean "Parker" spiral (Parker 1958); this field is dominated by the tangential component, while the radial component drops off as $1/r^2$. Also, the temperature is determined by adiabatic expansion of the wind, i.e. $V^{\gamma_{sw}-1}T = $ constant, where V is a volume element and γ_{sw} is the ratio of specific heats for the solar wind. We take $\gamma_{sw} = 5/3$ and assume that the termination shock is at 85 AU in all that follows. If, for example, we take values at 1 AU of $n_{p,AU} = 8$ cm^{-3}, $B_{AU} = 5\times10^{-5}$ G, $T_{p,\,AU} = 2 \times 10^5$ K, and $V_{sw} = 500$ km s^{-1}, we have for the termination shock parameters: $n_{p,TS} = 1.1 \times 10^{-3}$ cm^{-3}, $B_{TS} = 5.9 \times 10^{-7}$ G, $T_{p,\,TS} = 535$ K, and, for the Mach numbers, $\mathcal{M}_S \simeq 130$ and $\mathcal{M}_A \simeq 13$ ($\mathcal{M}_S$ is the sonic Mach number and $\mathcal{M}_A$ is the Alfvén Mach number). For this example, we have neglected pickup ions and ion species other than protons. The addition of pickup ions will lower $\mathcal{M}_S$ dramatically. We assume here and elsewhere that the electron and proton temperatures are equal, and that all ions have the same temperature per nucleon. This equality is used for its expediency and can, of course, be relaxed if data shows otherwise. In reality the electron component of the solar wind is somewhat hotter than the protons (e.g. see Baring et al. 1997), perhaps due

to their greater conductivity; large scale averages for electron temperatures are presented by Phillips et al. (1995).

We further assume a fixed value for Θ_{Bn}, repeating that our's is a plane shock model and can only describe a shock with a constant far upstream obliquity. We note that, while $d_{FEB} \ll D_{TS}$ in our models, the size of our system along the field lines, $d_{FEB} \tan\Theta_{Bn}$, is comparable to D_{TS} since $\Theta_{Bn} \lesssim 90°$. We do not model the range of magnetic field geometries around a spherical shock.

3.2. Pickup Ion Contribution to the Sonic Mach Number

Pickup ions contribute to the sonic Mach number $\mathcal{M}_S$ through both their mass loading of the solar wind, and also their velocity dispersion relative to the mean speed of the wind. This latter component is crucial to the determination of $\mathcal{M}_S$ at large distances from the sun, where adiabatic cooling of the solar wind has diminished its pressure below that of the pickup ions. The sound speed in the solar wind frame is

$$c_s = \sqrt{\frac{\partial P}{\partial\rho}} = \sqrt{\frac{\gamma P}{\rho}} , \quad \text{for} \quad P \propto \rho^\gamma \propto V^{1-\gamma} , \quad (5)$$

for a gas of one species (e.g. protons or helium ions), where γ is the ratio of specific heats for that species, P is the pressure, ρ is the mass density, and V is the volume. If the shock speed in the solar wind frame is V_{sk} ($\approx V_{sw}$), then the sonic Mach number is

$$\mathcal{M}_S = \frac{V_{sk}}{c_s} = \sqrt{\frac{d}{\gamma}} \frac{V_{sk}}{\sqrt{\langle v^2\rangle}} , \qquad (6)$$

where the pressure, $P = nm\langle v^2\rangle/d = \rho\langle v^2\rangle/d$, is expressed in terms of the mean of the square (i.e. dispersion) of the particle speeds v (measured in the solar wind frame). Here d is the dimensionality of the system. For a phase space speed distribution $f(v)$ of non-relativistic particles,

$$\langle v^2\rangle = \int_0^\infty v^4 f(v)\,dv \bigg/ \int_0^\infty v^2 f(v)\,dv . \qquad (7)$$

For a monoenergetic pickup ion injection distribution $f(v) = \delta(v - V_{sw})$, we have $\langle v^2\rangle = V_{sw}^2 (= V_{sk}^2)$, while for thermal solar wind particles with $\exp[-mv^2/(2kT)]$, the familiar result $\langle v^2\rangle = 3kT/m$ for a non-relativistic Maxwellian emerges.

To accommodate the two-component population of solar wind and pickup ions (denoted by subscripts "sw" and "pu," respectively), the speed of sound must by modified. Since pressures and densities add linearly, i.e. $P = P_{sw} + P_{pu}$ and $\rho = \rho_{sw} + \rho_{pu}$, then the adiabatic laws of

$$P_{sw}V^{\gamma_{sw}-1} = \text{const}_s \quad \text{and} \quad P_{pu}V^{\gamma_{pu}-1} = \text{const}_p \qquad (8)$$

can be used to derive

$$\begin{aligned}
c_s^2 &\equiv \frac{\partial P}{\partial\rho} = \frac{\partial P}{\partial V}\frac{dV}{d\rho} \\
&= -\left(\frac{\partial P_{sw}}{\partial V} + \frac{\partial P_{pu}}{\partial V}\right)\frac{V}{\rho} = \frac{\gamma_{sw}P_{sw} + \gamma_{pu}P_{pu}}{\rho_{sw} + \rho_{pu}} ,
\end{aligned} \qquad (9)$$

where γ_{sw} (γ_{pu}) is the ratio of specific heats for the solar wind (pickup ions). This exhibits an intuitive property, namely that the pressure terms can be added in the numerator and densities can be added in the denominator, imitating the situation for the spring constant and the mass in a harmonic oscillator. In general, $\gamma_{pu} \neq \gamma_{sw}$, and we observe that if the pickup ions maintain the two-dimensional ring distribution of their injection, as $\gamma = (d_{pu} + 2)/d_{pu}$, then one would obtain $\gamma_{pu} = 2$ for the pickup ion γ. Otherwise, if the pickup ions are isotropized, as will be assumed later in the paper, then $\gamma_{pu} = 5/3 = \gamma_{sw}$. It follows, that if d_{pu} and $\langle v^2 \rangle_{pu}$ are the dimensionality and mean square speed, respectively, of the pickup ions, then

$$\mathcal{M}_S = V_{sk} \left\{ \frac{5\, n_{sw} kT/m}{3\,(n_{sw} + n_{pu})} + \frac{d_{pu} + 2}{d_{pu}^2} \frac{n_{pu} \langle v^2 \rangle_{pu}}{n_{sw} + n_{pu}} \right\}^{-1/2} . \tag{10}$$

At the termination shock, the solar wind is very cold, so that the pickup ion component dominates the pressure, primarily because the pickup ion abundance is significant (for protons, beyond around 5 AU, the pickup ion density drops off roughly as $1/r$ since the accumulated injection of pick up ions scales more or less as r, which is diluted by the spherical expansion factor $1/r^2$; this contrasts the solar wind, whose density scales purely as the $1/r^2$ dilution factor). In this case,

$$\mathcal{M}_S \approx \sqrt{\frac{d_{pu}^2}{d_{pu} + 2} \frac{n_{sw} + n_{pu}}{n_{pu}} \frac{V_{sk}^2}{\langle v^2 \rangle_{pu}}} . \tag{11}$$

It follows that the dependence of the sonic Mach number on the dimensionality of the pickup ions is conveniently very weak, and that pickup ion abundances $n_{pu}/(n_{sw} + n_{pu})$ exceeding around 1%, limit the Mach number to around ten. As one moves from 1AU towards the termination shock, adiabatic cooling of the solar wind forces $\mathcal{M}_S$ to increase slowly ($\propto r$) until the pickup ions dominate the pressure and the Mach number saturates at the above value.

In all that follows, we take $d_{pu} = 3$ and calculate $\langle v^2 \rangle_{pu}$ directly from the injected pickup distributions assuming they are isotropic in the local frame.

3.3. Adiabatic Evolution of the Pickup Ion Distribution

As the solar wind expands in its progression to the outer heliosphere, it cools as does the pickup ion distribution. The pickup ions are, however, continually injected at rates depending on their distance from the sun, so the determination of their distribution at the termination shock is non-trivial. The calculation of the injection rates and resulting distribution function depends on details such as the radial variations of the ionizing solar UV flux and solar wind density, and the gravitational focusing of interstellar neutrals in the inner heliosphere. We use a standard expression for the pickup ion phase-space distribution, $f_{pu}(r, v)$, in the solar wind frame, in the nose region of the termination shock (e.g. Gloeckler et al. 1993, 1994; le Roux, Potgieter, & Ptuskin 1996), for a *three-dimensional* isotropic population, based on the derivation of Vasyliunas

& Siscoe (1976):

$$f_{pu}(r, v) = \frac{3}{8\pi} \left(\frac{u_\infty}{V_{sw}^4} \right) \left(\frac{\Lambda}{r} \right) \left(\frac{v}{V_{sw}} \right)^{-3/2} n(r, v)\, \Theta(V_{sw} - v), \tag{12}$$

where v is the particle speed, r is the radial distance (of the termination shock in this application) from the sun along the line pointing toward the nose of the termination shock, and $u_\infty \simeq 20$ km s^{-1} is the velocity of the Sun relative to the local interstellar medium. Here $\Lambda = \nu_E r_E^2/u_\infty$ is the characteristic ionization distance for interstellar neutrals, where ν_E is the frequency of ionization at the Earth, i.e. at a radial distance of $r_E = 1$ AU from the Sun. While Λ is written in terms of quantities measured at 1 AU, it is actually independent of radius due to the $1/r^2$ decline in the solar wind density (which is involved in charge exchange with the interstellar neutrals) and the ionizing solar UV flux. The values we adopt for the ionization frequencies of various ionic species at Earth are taken from the determinations at solar minimum of Rucinski, Fahr, & Grzedzielski (1993), and were those used by le Roux, Potgieter, & Ptuskin (1996), namely $\nu_E = 5 \times 10^{-7}$ s^{-1}, 6.7×10^{-8} s^{-1}, and 5×10^{-7} s^{-1} for hydrogen, helium, and oxygen, respectively. These values differ significantly (at least for hydrogen and helium) from the earlier values quoted by Vasyliunas & Siscoe (1976) and fall below the mean ionization frequencies recorded over the entire solar cycle by factors of around 1.5 (e.g. Rucinski et al. 1996). The Heaviside step function $\Theta(V_{sw} - v)$ is unity for non-negative arguments and zero otherwise, so that it cuts the distribution off at the solar wind speed, V_{sw}. The factor $n(r, v)$ in Equation (12) is given in terms of the neutral density in the interstellar medium, n_∞, by:

$$n(r, v) = \frac{n_\infty}{4\chi}(1 + \chi)^2 \exp\left\{ -\left(\frac{\Lambda}{r} \right)\left(\frac{v}{V_{sw}} \right)^{-3/2} \frac{2}{|1 + \chi|} \right\}, \tag{13}$$

with

$$\chi^2 = 1 - \frac{r_p(0)}{r} \left(\frac{v}{V_{sw}} \right)^{-3/2} , \tag{14}$$

and

$$r_p(0) = 2GM_\odot(\mu - 1)/u_\infty^2 . \tag{15}$$

In these expressions, G is the gravitational constant, $M_\odot$ is the mass of the Sun, and μ is the ratio of the solar radiation pressure to the solar gravitational force. Hence $r_p(0)$ is the negative (for $\mu \leq 1$) of the radius where the gravitational potential (suitably modified for radiation pressure) equals the kinetic energy of the interstellar neutrals, i.e. approximately where gravitational deflection of neutrals becomes important. Note that, except for the step function, the particle speed v and the radial distance r in Eqs. (12)–(13) always appear in the combination $r_i \equiv (v/V_{sw})^{3/2} r$, which is just the radius of injection of pickup ions that adiabatically cool to speed v at radius r. Therefore, if $n(r, v)$ is expressed as a function of r_i, n represents the density of neutrals at the radius r_i of injection. These characteristics of adiabatic evolution of the pickup ion distribution were established by Vasyliunas & Siscoe (1976), who also presented results for two-dimensional pick-up ion populations.

Except for minor changes in notation, the above expressions are taken directly from le Roux, Potgieter, & Ptuskin (1996), and following them, we use $\mu = 0.7$ for hydrogen and $\mu = 0$ for helium and oxygen to generate the pickup ion distributions. For our comparisons with the ACR observations presented in Cummings & Stone (1996), we normalize the pickup distributions generated with the above equations to the densities estimated by Cummings and Stone.
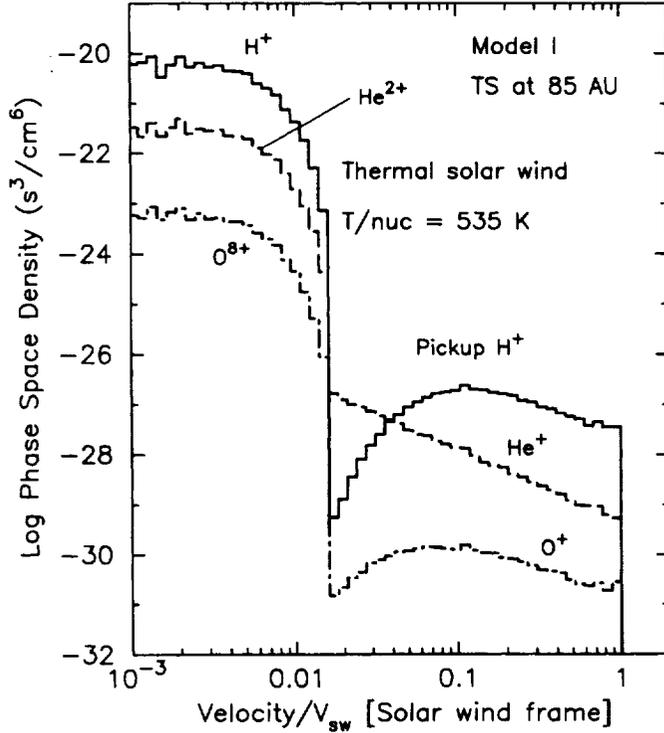

FIG. 1.— Upstream Phase-space densities for pickup ions expected at 85 AU calculated using equations (12) and (13) with $n_\infty(H) = 0.077$, $n_\infty(He) = 0.01$, $n_\infty(O) = 9.7 \times 10^{-5}$ cm^{-3}. The velocity is in units of the solar wind speed, V_{sw}. The three thermal ion species are all injected with a temperature per nucleon of 535 K with charge states: H$^+$, He^{2+}, and O^{8+}. The pickup ions have a charge state of $+1$. The flat nature of the He$^+$ distribution relative to those of H and O reflects its much longer ionization length.

3.4. Direct Acceleration of Anomalous Cosmic Rays at the Termination Shock

We now present a model for the acceleration of anomalous cosmic ray H$^+$, He$^+$, and O$^+$. Using the observations of Geiss et al. (1994) and the model of Vasyliunas & Siscoe (1976) just discussed, Cummings & Stone (1996) estimate the following pickup ion fluxes at the nose of the heliosphere: $F_p^{pu} \simeq 1.0 \times 10^4$ cm^{-2} s^{-1}, $F_{He}^{pu} \simeq 230$ cm^{-2} s^{-1}, and $F_O^{pu} \simeq 5.3$ cm^{-2} s^{-1}. Again assuming that the solar wind speed is constant and equal to 500 km s^{-1}, the pickup densities at the termination shock are then: $n_p^{pu} \simeq 2 \times 10^{-4}$ cm^{-3}, $n_{He}^{pu} \simeq 4.6 \times 10^{-6}$ cm^{-3}, and $n_O^{pu} \simeq 1.1 \times 10^{-7}$ cm^{-3}. These values correspond to $n_\infty(H) = 0.13$ cm^{-3}, $n_\infty(He) = 0.02$ cm^{-3}, and $n_\infty(O) = 7 \times 10^{-5}$ cm^{-3}, somewhat different from the values assumed by le Roux, Potgieter, & Ptuskin (1996). More recently, Gloeckler, Fisk, & Geiss (1997) report $n_\infty(H) = 0.115$ cm^{-3} and

$n_\infty(He) = 0.0153$ cm^{-3}. These differences are relatively small and we use the Cummings and Stone values to allow for a direct comparison. The values are listed in Table 1 under Model I along with corresponding solar wind values at the Earth, for densities, temperatures, and the estimated magnetic field strength. We assume $\Theta_{Bn} = 89°$, inject the thermal and pickup ions with far upstream (i.e. $-x \gg \eta r_{g1}$, where $r_{g1} \equiv m_p V_{sk} c/e$) phase space distributions as shown in Figure 1, and use $\eta = 14$, chosen to give a good fit to the observed ACR intensities, as will become evident shortly.

TABLE 1
PARAMETERS FOR TERMINATION SHOCK MODELS

Parameters[a]	Model I	Model II	Model III
V_{sk} [km s^{-1}]	500	500	360
Θ_{Bn}	89°	80°	87°
B_{TS} [G]	5.9×10^{-7}	5.9×10^{-7}	8×10^{-7}
η	14	35	5
Hydrogen			
$n_{p,AU}$ [cm^{-3}] [b]	8	8	2.5
$n_{p,TS}$ [cm^{-3}]	1.1×10^{-3}	1.1×10^{-3}	3.44×10^{-4}
n_p^{pu} [cm^{-3}] [c]	2.0×10^{-4}	2.0×10^{-4}	2.43×10^{-4}
Helium			
$n_{He,AU}$ [cm^{-3}] [b]	0.4	0.4	0.12
$n_{He,TS}$ [cm^{-3}]	5.5×10^{-5}	5.5×10^{-5}	1.72×10^{-5}
n_{He}^{pu} [cm^{-3}] [c]	4.6×10^{-6}	4.6×10^{-6}	5.65×10^{-6}
Oxygen			
$n_{O,AU}$ [cm^{-3}] [b]	8×10^{-3}	8×10^{-3}	2.5×10^{-3}
$n_{O,TS}$ [cm^{-3}]	1.1×10^{-6}	1.1×10^{-6}	3.44×10^{-7}
n_O^{pu} [cm^{-3}] [c]	1.1×10^{-7}	1.1×10^{-7}	1.34×10^{-7}
$\mathcal{M}_S$	5.2	5.2	3.1
$\mathcal{M}_A$	15.4	15.4	5.4
r	3.54	3.54	2.77
d_{FEB} [λ_0] [d]	274	1100	4030
d_{FEB} [AU] [d]	2.3	23	6.3
λ_0 [AU]	8.3×10^{-3}	0.02	1.6×10^{-3}
$2d_\parallel/(\pi R_{sk})$	0.98	0.97	0.91

NOTE.— (a) All models assume that the shock is at 85AU and that the temperature per nucleon at 1 AU is 2×10^5 K and is ~ 500 K at the termination shock for all ion species. In all cases, the electron temperature is set equal to the proton temperature. (b) The solar wind values assumed for Models I and II give the ratios, $n_{p,AU}/n_{He,AU}/n_{O,AU} = 1/0.05/0.001$, which are close to normal solar wind values (e.g. Ipavich et al. 1988 and references therein). (c) The pickup ion values we use for Models I and II are from Cummings & Stone (1996) who give the ratios: 5.3/228/10240 for pickup O/He/H number fluxes (in units of cm^{-2} s^{-1}). For $V_{sk} = 500$ km s^{-1}, these give the number densities shown. The pickup ion densities for Model III are set to give the same He$^+$/H$^+ \simeq 43$ and O$^+$/H$^+ \simeq 1800$ ratios as Models I and II. (d) These values of d_{FEB}, listed both in units of λ_0 and AU, are chosen to yield proton turnover energies near 150 MeV. The parameter $\lambda_0 = \eta r_{g1}$ is calculated using B_{TS}.
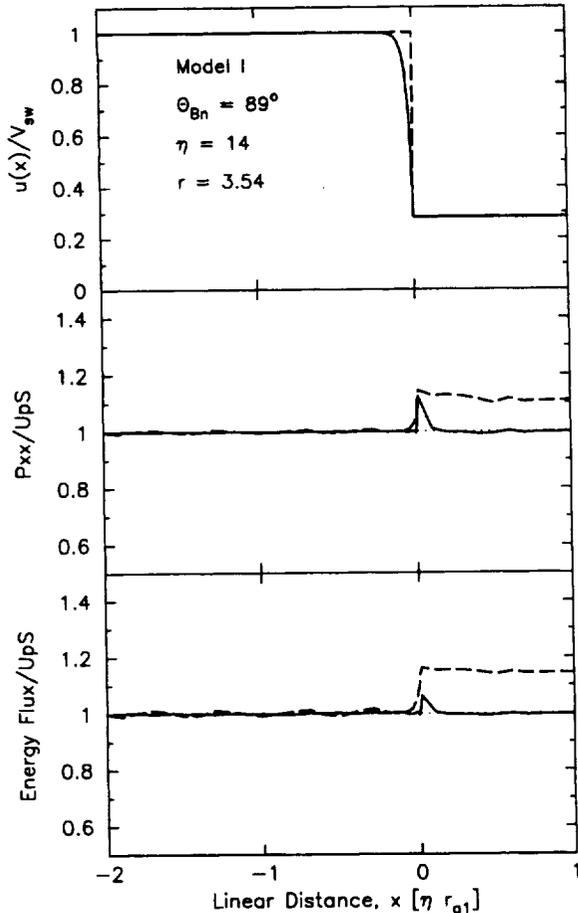
FIG. 2.— Determination of shock structure by iteration. The top panel shows the x-component of the flow speed, $u_x(x)$, the middle panel shows the xx-component of momentum flux, and the bottom panel shows the energy flux, all normalized to far upstream values. In each panel, the first and last iterations are shown as dashed lines and solid lines, respectively. The energy and momentum fluxes are conserved throughout the shock to within 1%.

The self-consistent shock profile is shown as a solid line in the top panel of Figure 2, along with the xx-component of the momentum flux and the energy flux in the lower two panels. In each panel, the dashed line is the test-particle quantity obtained with the discontinuous shock and the solid line is the value obtained after the self-consistent smooth shock structure has been found. For a complete description of how the shock structure is determined, see Ellison, Baring, & Jones (1996). The important point is that, even for an obliquity of 89°, the injection and acceleration of thermal and pickup ions is efficient enough to cause some departures from momentum and energy conservation in the discontinuous shock; the downstream fluxes rise to a factor of > 1.1 above the far upstream values. Even though the shock smoothing is quite small (Figure 2 uses a linear distance scale and the portion of the shock shown is a small fraction of the size set by $d_{\rm FEB}$), it is necessary to conserve momentum and energy fluxes. Our self-consistent, smooth shock solution conserves all fluxes, including the zz-component of momentum and uniformity of the tangential electric field (not shown), across the shock. The angle between the shock normal and the

magnetic field goes smoothly from $\Theta_{\rm Bn} = 89°$ far upstream to $\Theta_{\rm Bn} = 89.72°$ downstream. The addition of the pickup ions has caused the sonic Mach number to decrease substantially from the example we gave above, i.e. here $\mathcal{M}_{\rm S} = 5.2$ versus $\mathcal{M}_{\rm S} = 130$ without pickup ions (see Table 1).

Note that even though $d_{\rm FEB}$, which is measured along the shock normal, may be a small fraction of the shock radius, the high obliquity means that ions will move much greater distances along the shock face. Setting the distance parallel to the shock face in our plane-shock approximation to be $d_\| \sim d_{\rm FEB} \tan \Theta_{\rm Bn}$, we require for consistency that particles stream no more than the pole-to-equator distance, i.e.

$$d_\| < \pi R_{\rm sk}/2 , \tag{16}$$

or,

$$d_{\rm FEB} \lesssim \frac{\pi R_{\rm sk}}{2 \tan \Theta_{\rm Bn}} . \tag{17}$$

Clearly, the quasi-spherical geometry of the termination shock renders the effective value of $d_\|$ somewhat (but not much) less than the bound in equation (16). The quantity, $2d_\|/(\pi R_{\rm sk})$ is listed in Table 1 and for this example (Model I), $2d_\|/(\pi R_{\rm sk}) \simeq 1.1$.

In Figure 3 we show the model spectra, calculated at the termination shock, along with Voyager 1 (V1) data measured (well within the termination shock) during 1994 on days 157-313 (Cummings & Stone 1996; see also Christian, Cummings, & Stone 1995). The value of η has been chosen to obtain general agreement with the normalization of the ACR proton observations, but there has been no other adjustment of normalization in the top panel. Smaller values of η (i.e. stronger scattering) would yield higher model intensities at ACR energies (i.e. in conflict with the data) and larger values would yield lower model intensities. Note that the intensity of the ACR H^+ peak at ~ 50 MeV is ~ 10 orders of magnitude below the H^+ pickup bump at ~ 2 keV; only a tiny fraction of pickup ions need to be accelerated to energies above ~ 10 MeV to account for the observed ACR fluxes. The value of $\eta = 14$ used to obtain the "fit" should be regarded only as a rough indication of the true value, given the sensitivity of the ACR flux to the pick-up ion abundance and the shape of their distribution.

In examining Figure 3 it must be remembered that the V1 observations were made at an average radial location of 57 AU and show the effects of solar modulation. Our model spectra, on the other hand, are calculated at the termination shock and do not include modulation. Note that our shock acceleration simulation does generate low energy "modulation-like" depletions in upstream populations (e.g. Baring, Ellison, & Jones 1994; Ellison, Baring, & Jones 1996) due to inefficient convection against the fluid flow, much like the model of Lee (1982). However, for the termination shock models of this paper, such depletions appear relatively close to the shock, on scales $\ll D_{\rm TS}$, due to our incomplete modeling of particle convection and diffusion in the complex geometry of the heliosphere. The heavy solid line in Figure 3 is the estimate of Cummings & Stone (1996) for the power law H^+ spectrum at the termination shock and, as mentioned above, we have chosen η to approximately match this intensity (fine tuning of η would give a more precise match).
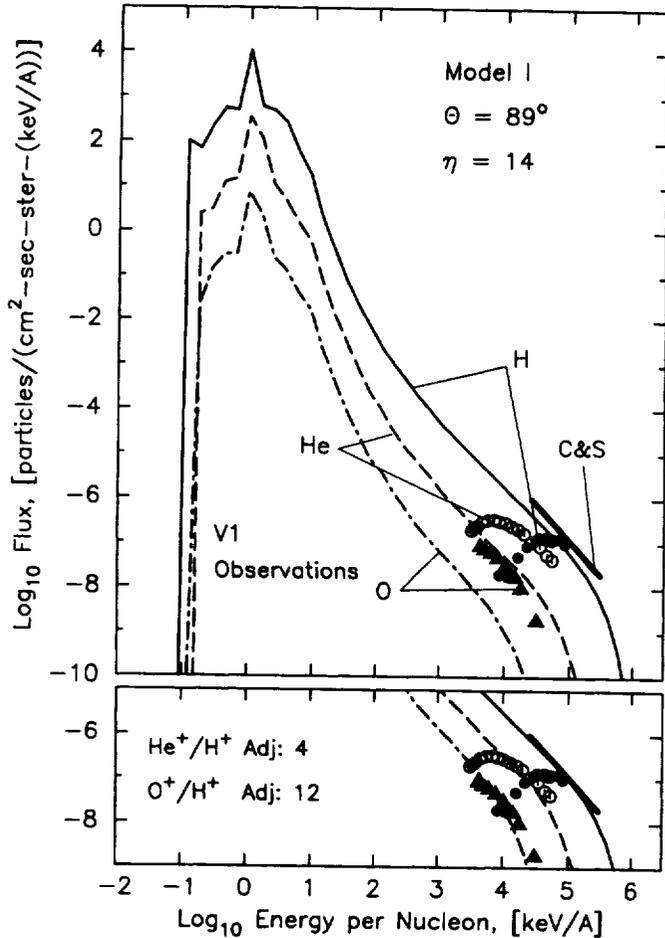
FIG. 3.— Comparison of Voyager 1 observations of ACR H, He, and O (made during 1994/157-313 when V1 was at an average radial location of ~ 57 AU) to Model I spectra calculated *at the termination shock*. The model spectra have an absolute normalization determined by the injection parameters, i.e. $n_{\rm p,TS} V_{\rm sw} = 5.5 \times 10^4$ cm^{-2} s^{-1} for the protons and corresponding values for the He and O. The value of η has been chosen to give a general fit to the intensities of the observed ACR's. The sharp thermal peaks show the relatively cold solar wind ions that have not yet thermalized. As the observation position is moved downstream, these peaks broaden. Note that the H thermal peak intensity is ~ 11 orders of magnitude above the observed ACR intensity. The heavy solid line is the Cummings & Stone (1996) estimate for the ACR proton intensity at the termination shock. In the bottom panel, we have individually adjusted the normalizations to match the ACR observations. The relative adjustments for He$^+$ and O$^+$ are labeled.

There are several points to consider. First, the limits on the maximum ACR energy are such that the Cummings & Stone extrapolation extends into the exponential cutoff. Second, even though the shock model we are using has a compression ratio of $r = 3.54$, well above that inferred by Cummings & Stone, the spectral *slope* in the very limited energy range (i.e. above the modulation turnover) provided by the data is reasonably well fit. Because of the limited energy range and the spectral cutoff, it may not be possible to meaningfully constrain the termination shock Mach number by extrapolating ACR observations made well inside the heliosphere back to the termination shock as done by Cummings & Stone (1996). Third, the ACR data clearly show that the observed He$^+$/H$^+$ ratio is greater than our model predicts. This is also true for the O$^+$/H$^+$ ratio and in order to match the observed fluxes,

we would have to increase, relative to H, the He$^+$ intensity by a factor ~ 4, and the O$^+$ intensity a factor ~ 12. This adjustment has been done in the bottom panel of Figure 3 to show that the shapes of the observed ACR spectra are matched exceeding well by our model above the modulation turnover. In particular, our single parameter $d_{\rm FEB}$, simultaneously gives a good match to the cutoff for all three species.

Considering the uncertainties involved in estimating the various parameters needed at the termination shock, such as the solar wind speed and the pickup ion densities, we believe the match indicated in Figure 3 is acceptable.
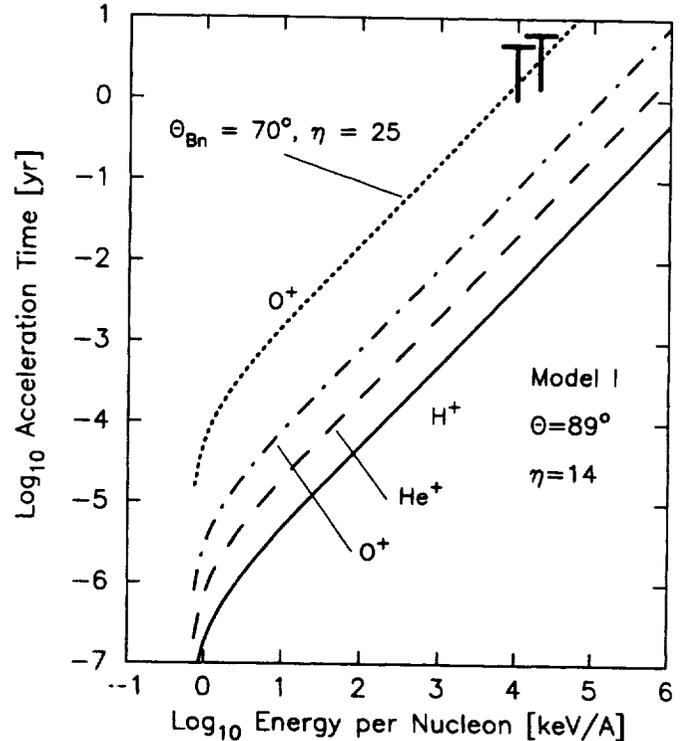

FIG. 4.— Acceleration time in years versus energy per nucleon for the H$^+$ (solid line), He$^+$ (dashed line), and O$^+$ (dot-dashed) produced in Model I. These curves are calculated from the analytic result given in Ellison, Baring, & Jones (1995). The upper limits on the O acceleration time from electron stripping at 10 and 20 MeV/A are from Adams & Leising (1991). The 70°, $\eta = 25$ curve is included to indicate what shock parameters are necessary to encroach upon the experimental upper limits.

3.4.1. Acceleration Time

An important constraint on the production of ACRs comes from the charge stripping rate; clearly considerations of ACR generation are simplified when charge-stripping timescales exceed those of acceleration. Such ionization is relevant to species heavier than He (whose stripping timescales are long), in this case oxygen. Adams & Leising (1991) showed that 10 MeV/A singly charged oxygen ions will be further stripped, in conflict with observations, if they propagate more than ~ 0.2 pc in the local interstellar medium. Jokipii (1992) showed how this relates to the acceleration rates of various mechanisms, and concluded that first-order Fermi acceleration at highly oblique shocks is the only mechanism fast enough to satisfy this limit. Our results are in agreement with this assess-

ment and we plot the acceleration time versus energy per nucleon in Figure 4 for our Model I. Here, the dot-dashed line is O^+, the dashed line is He^+, and the solid line is H^+. The plots in Figure 4 were calculated using the analytic result of Ellison, Baring, & Jones (1995) [i.e. equation (4) of that paper with $E_i = 0.6$ MeV/A], but our direct Monte Carlo determination of the acceleration time is consistent with this at superthermal energies, as also shown in Ellison, Baring, & Jones (1995).

The actual limits of 4.6 and 6.3 yrs placed on the propagation of oxygen by Adams & Leising (1991) are shown as upper limits at 10 and 20 MeV/A, respectively. The acceleration time is well below these limits, though we also depict a 70°, $\eta = 25$ case to indicate what type of shock parameters might be needed for charge stripping to be relevant. In addition to the limits of Adams & Leising, there is also the report of observations of ACR oxygen in higher ionization states than O^+ (Mewaldt et al. 1996), a constraint that provides a lower limit to the diffusive acceleration timescale. Given that such energies per nucleon are at the upper end of the oxygen spectrum in the models presented here (e.g. see Figure 7 below), it appears that detailed consideration of ACR propagation and diffusion in the heliosphere is necessary to obtain a suitable description of energetic oxygen in various ionization states. As mentioned above, we have not included charge stripping in our present calculation, but will include this effect in future work. We remark that Jokipii (1996) has included electron stripping in his acceleration and transport model and finds good agreement with these observations.

3.5. Limited Parameter Survey

3.5.1. Variation of Θ_{Bn}

It is instructive to explore how our model output changes with variations in its most important parameters, namely η and Θ_{Bn}. In Model II we have changed Θ_{Bn} from 89° to 80° to see the effect this has on our fits to the ACR observations. We have kept all other input parameters the same as in Model I except that we have altered η to give a general fit to the H ACR intensity as before. The injection efficiency depends strongly on both η and Θ_{Bn} (e.g. Ellison, Baring, & Jones 1995), increasing as either Θ_{Bn} or η is decreased. By decreasing Θ_{Bn} from 89° to 80°, we must reduce the scattering efficiency (in this case by setting $\eta = 35$) to obtain a fit to the ACR H^+ intensities. Once this adjustment is made, the characteristics of the 80° and 89° results are similar as is shown in Figure 5, where we compare the proton spectra from Model I (solid line) and the 80° example, Model II (dashed line). While η has changed compared to Model I, the maximum energy has been kept essentially the same by varying d_{FEB}. Of course we do not answer (or even address) the question of how the magnetic turbulence is produced, or why it obtains a level which gives observed ACR intensities (i.e. why η has a particular value). However, this example does show that the injection process is perfectly well defined within standard diffusive shock acceleration and that a smooth change in parameters results in a continuous change in output efficiencies.
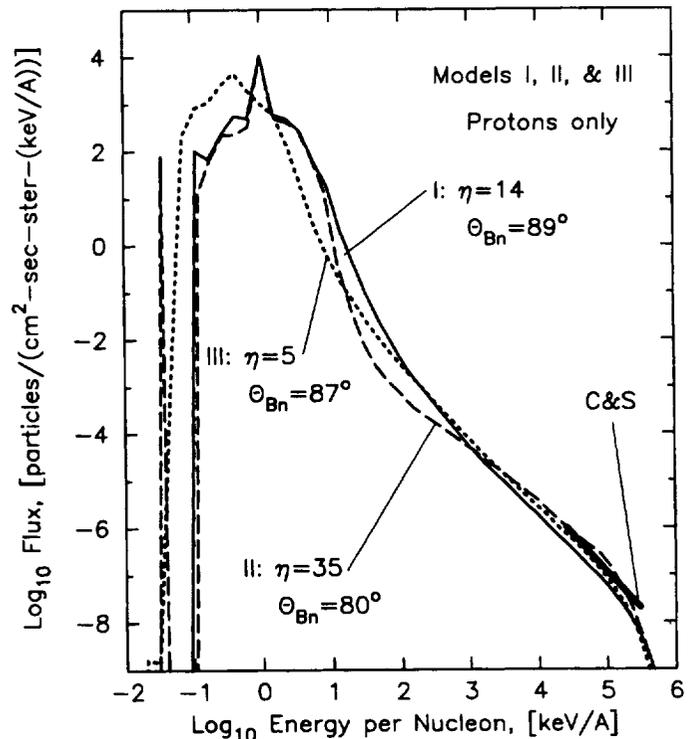

FIG. 5.— Comparison of the proton spectra for Models I (solid line), II (dashed line), and III (dotted line), illustrating the variation of model output with shock obliquity (comparing Models I and II) and shock strength (Model I vs. III), keeping the 10 MeV/A ACR flux more or less constant by adjusting the value of η. The heavy solid line is the Cummings & Stone (1996) estimate for the ACR proton power-law intensity at the termination shock. Fine tuning of η would allow a more exact match between our models and the Cummings & Stone intensity.

It is also true that if Θ_{Bn} is decreased much below 80°, the value of η required to obtain the observed ACR intensity will become so large that the size of the foreshock region is greater than the termination shock radius or that $d_\parallel > \pi R_{sk}/2$. Note from Table 1 that d_{FEB} goes from 2.3 AU for Model I to 23 AU for Model II. This suggests that, at least within the simple assumptions we have made here, the termination shock cannot be injecting and accelerating pickup ions for significant times in states where the local $\Theta_{Bn} \lesssim 70°$. In order to match the ACR intensities, the increased injection resulting from the low obliquity must be matched by a decrease in scattering efficiency which implies length scales which are inconsistent with the size limitations of the termination shock. It may be possible, however, that large departures from highly oblique conditions last for short times (e.g. Kucharek & Scholer 1995), but if these conditions result in enhanced injection, as has been suggested, the time-averaged η must be correspondingly increased to satisfy the observed ACR intensities. The time needed to accelerate ions to ACR energies will also increase as Θ_{Bn} is decreased and η is increased. The dotted line in Figure 4 shows the acceleration time for O^+ when $\Theta_{Bn} = 70°$ and $\eta = 25$. While this is still consistent with the upper limits of Adams & Leising (1991), it does suggest that a much larger fraction of ACRs will be multiply charged if non-highly oblique portions of the termination shock contribute significantly to the observed ACRs.

3.5.2. Low Mach Number Example and Effect of Pickup Ions

The models we have used so far have all had sonic Mach numbers $\mathcal{M}_S \gtrsim 5$ and compression ratios $r \gtrsim 3.5$. These compression ratios are considerably larger than the $r \sim 2.6$ estimated by Stone, Cummings, & Webber (1996) and Cummings & Stone (1996) from the ACR spectral shapes, but they are what would be expected for a solar wind speed of ~ 500 km s^{-1} and the densities estimated by Cummings & Stone. To investigate the effect of Mach number, we have performed another simulation where we have modified our parameters to yield a weaker shock, i.e. $r \simeq 2.8$. We use a smaller solar wind speed at the termination shock, i.e. $V_{sk} = 360$ km s^{-1} (as estimated by Isenberg 1997), and have adjusted our solar wind and pickup ion densities and other parameters (e.g. $\Theta_{Bn} = 87°$) as indicated by Model III in Table 1, to maintain $d_{\parallel} \sim \pi R_{sk}/2$. As before, we iterate to a self-consistent shock structure after adjusting η to give a reasonable fit to the ACR intensity.

a good match to the ACR observations as shown in Figure 6. Any small discrepancies between this model (or the others) and the ACR H$^+$ intensity (extrapolated by Cummings & Stone) can be removed by fine tuning η. The difficulty in deducing the shock strength from the spectral shape (which is strongly influenced by the non-linear shock smoothing) in the limited energy range afforded by the ACRs is also obvious from this Figure.
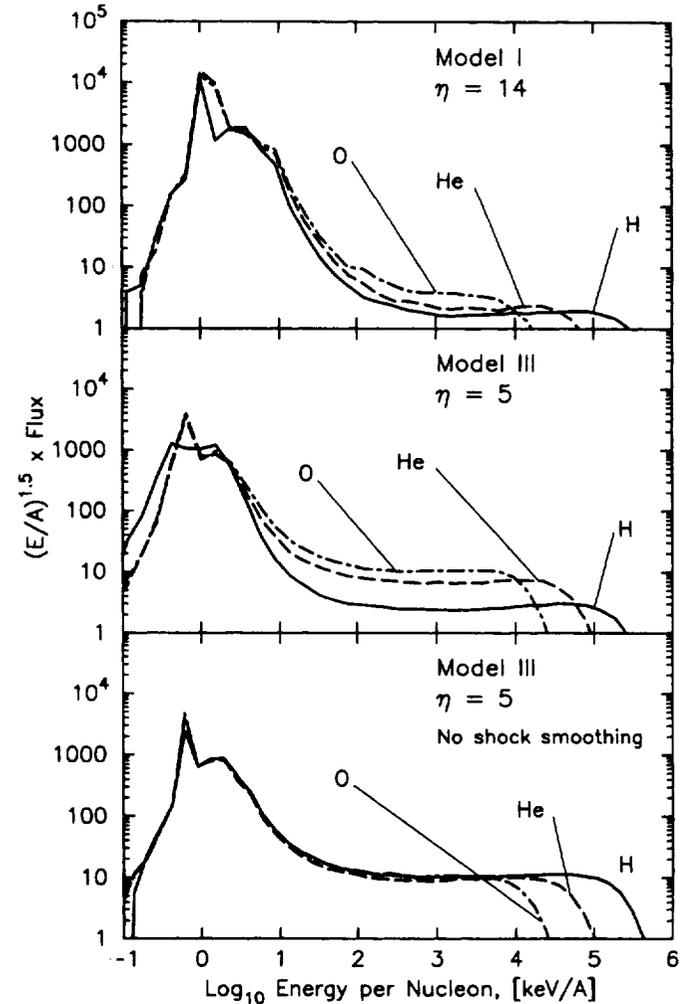
FIG. 7.-- Spectra from Models I and III renormalized and multiplied by $(E/A)^{1.5}$. In each case, we have normalized all spectra to the same pickup ion density, i.e. for Model I we have multiplied the He spectrum by $n_p^{pu}/n_{He}^{pu} \simeq 43$ and the oxygen by $n_p^{pu}/n_O^{pu} \simeq 1800$, and for Model III, we have multiplied the He spectrum by $n_p^{pu}/n_{He}^{pu} \simeq 170$ and the oxygen by $n_p^{pu}/n_O^{pu} \simeq 7000$. In the top two panels, the self-consistent smooth shock is used to produce the spectra and a clear A/Q enhancement of He$^+$ or O$^+$ to H$^+$ is seen. In the bottom panel, we determined the spectra using the test-particle, discontinuous shock and essentially no enhancement (other than statistical variations) is present.
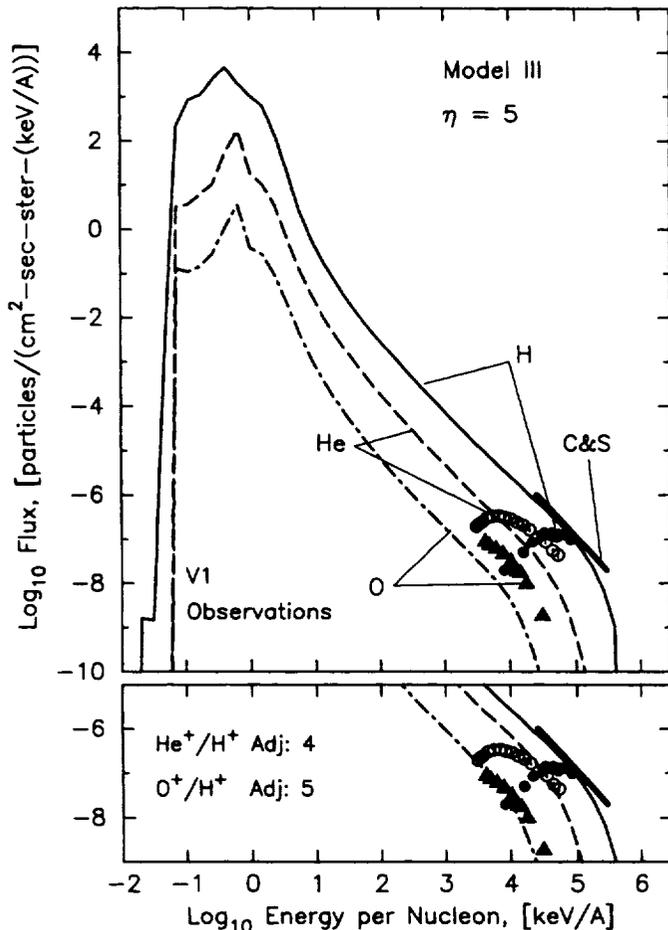

FIG. 6.— Same as Figure 3 for Model III. As in Figure 3, in the bottom panel we have individually adjusted the normalizations to match the ACR observations. The relative adjustments for He$^+$ and O$^+$ are labeled.

The low compression ratio produces a steeper spectrum than in our previous examples, and in order to match the ACR intensity at ~ 100 MeV, a larger injection efficiency (i.e. smaller η) is required. We find that $\eta \simeq 5$ yields

It has been known for some time that the acceleration efficiency of shocks that are smoothed by the pressure of accelerated particles is an increasing function of A/Q (e.g. Eichler 1979; Ellison, Jones, & Eichler 1981; see Ellison, Drury, & Meyer 1997 for a recent reference) in quasi-parallel scenarios. This effect, which depends only on the conservation of momentum and a spatial diffusion

coefficient which is an increasing function of energy, occurs because non-relativistic ions with larger A/Q (i.e. larger rigidities) have longer upstream diffusion lengths, at a given energy per nucleon. The fact that the shock is smoothed means that the high A/Q particles 'feel' a larger effective compression ratio and are accelerated more efficiently and, the greater the smoothing, the greater the enhancement. Enhancements have been confirmed at the quasi-parallel Earth bow shock (i.e. Ellison, Möbius, & Paschmann 1990) and should occur regardless of the shock obliquity *as long as the shock is smoothed*. In order to investigate this A/Q enhancement, we re-plot the model spectra from Figures 3 and 6, renormalizing the helium and oxygen spectra so they have the same upstream pickup ion number density as hydrogen, so that any difference produced during acceleration can be seen directly. That is, for both Models I and III, we multiply the helium by $n_p^{pu}/n_{He}^{pu} \simeq 43$ and the oxygen by $n_p^{pu}/n_O^{pu} \simeq 1800$.
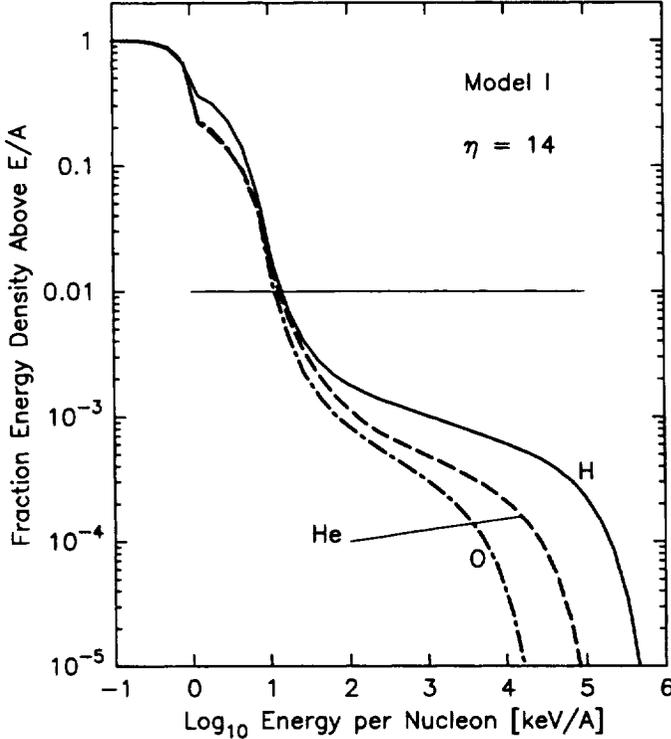

FIG. 8.— Acceleration efficiency in terms of the fraction of energy density in ions with energy per nucleon E/A and above. The solid, dashed, and dot-dashed curves are the H, He, and O efficiencies determined from Model I. Intercepts with the horizontal line show the energy per nucleon where each species is 1% efficient.

The results are shown in the top two panels of Figure 7 with all spectra multiplied by $(E/A)^{1.5}$. Both Models show an A/Q enhancement effect and although it is somewhat larger in Model III than Model I, it is still not as strong as deduced by Cummings & Stone (1996). The bottom panel of Figure 7 shows Model III with no shock smoothing but all other parameters the same. Here, there is essentially no difference in the various spectra, other than at the high energy turnover, as expected. As indicated in the lower panel of Figure 6, our Model III He$^+$/H$^+$ and O$^+$/H$^+$ ratios are still lower than the observed ACR ratios by a factor of ~ 5. The actual acceleration efficiency $\epsilon(E/A>)$

for Model I, as defined above to be the fraction of energy density in particles of energy per nucleon E/A and above, is shown in Figure 8. From this we see that 1% of the energy density (horizontal line) lies above ~ 10 keV/A for all three species. Note that at high energy per nucleon, the protons dominate (see also Figure 7) because they extend to higher E/A for a given gyroradius.
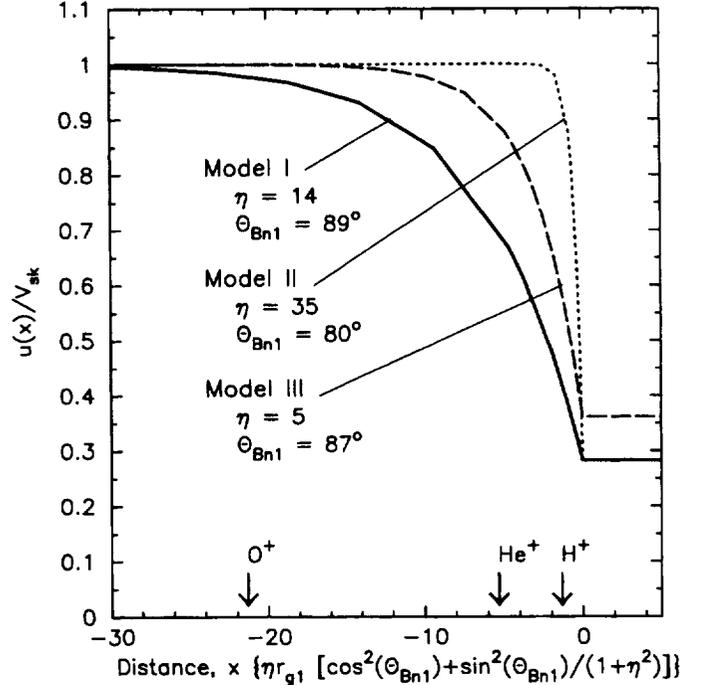

FIG. 9.— Shock profiles [i.e. $u(x)/V_{sk}$] for models I, II, and III. Note that the different values of $u(x)/V_{sk}$ in the downstream region (i.e. $x > 0$) result from different compression ratios. The abscissa is scaled in units of the upstream diffusion length (times 3) for protons travelling with the solar wind speed (see Equation [18]). The arrows at the bottom denote the different *upstream* scalelengths for diffusion of the three pickup species, obtained by setting $v = V_{sw}$ in Equation (18).

The somewhat larger A/Q enhancement of Model III compared to Model I may arise due to the different shock structures for these models; these are exhibited in Figure 9. In comparing smoothing in the various models, it is instructive to scale the distance normal to the shock in units of the diffusion length in the normal direction. For field obliquity Θ_{Bn}, the diffusion coefficient in this direction is $\kappa_{xx} = \kappa_\parallel \cos^2 \Theta_{Bn} + \kappa_\perp \sin^2 \Theta_{Bn} = \kappa_\parallel [\cos^2 \Theta_{Bn} + \sin^2 \Theta_{Bn}/(1 + \eta^2)]$ using kinetic theory to relate $\kappa_\perp$ to $\kappa_\parallel$. It then follows, using the scaling units of $r_{g1} = m_p V_{sw} c/e$, that the diffusion length κ_{xx}/V_{sw} is given by

$$\frac{\kappa_{xx}}{V_{sw}} = \frac{1}{3} \frac{A}{Q} \left(\frac{v}{V_{sw}}\right)^2 \eta r_{g1} \left\{\cos^2 \Theta_{Bn} + \frac{\sin^2 \Theta_{Bn}}{1 + \eta^2}\right\} \quad (18)$$

for particles of speed v. The factor in curly brackets times ηr_{g1} is used as the length unit in Figure 9. Hence the Figure gives an indication of the relative smoothing incurred in the different models. Model I is smoother than Model III which seems in conflict with the fact that Model III shows a larger A/Q effect. This behavior indicates the complexity of such highly oblique systems, which will de-

pend on other factors such as the shock speed, Mach number, the total compression ratio, and pick-up ion abundances. Furthermore, the spectra in Figure 7 indicate that Model III is a more efficient injector than Model I, a property which follows from the sharper nature of the Model III profile. In Figure 9, arrows mark the typical upstream diffusion scales of the three pick-up ion species (relative to the shock), determined by setting $v = 2V_{sw}$ in Equation (18). These will be somewhat modified in the downstream region due to the different field obliquity there. The diffusion lengths indicate that little A/Q enhancement would be expected for Model II, and that most should be seen for Models I & III, given that helium and oxygen pickup ions sample much larger compression ratios than hydrogen in these two cases. The interpretation of the A/Q enhancement is further complicated by the fact that diffusion in the downstream region (whose scales are not exhibited in the Figure) modifies the typical scalelengths, and that this depends in a complicated manner on the values of Θ_{Bn}, η, the Mach number, and the overall compression ratio. We remark that such complexities of A/Q enhancement behavior are diminished in strong shocks and particularly in quasi-parallel ones, where the number of influential shock parameters is reduced.
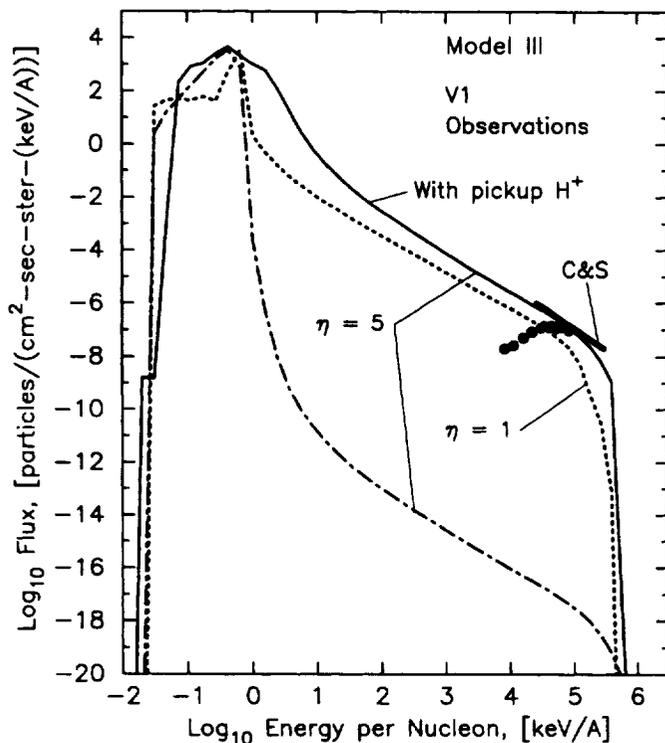

FIG. 10.— The solid line is the same proton spectrum shown in Figure 6, as are the ACR proton data and the Cummings and Stone extrapolation. The dotted and dot-dashed lines are calculated with no pickup ions for the two values of η shown. Injection is extremely sensitive to η, but for scattering at the Bohm limit ($\eta = 1$), ACR intensities can be produced at the termination shock with only thermal solar wind ions.

Even though we have had to make some changes in Model III from our previous examples to reduce $2d_\parallel/(\pi R_{sk})$ to ~ 1 (we have increased B_{TS} to 8×10^{-7} G and lowered Θ_{Bn} to 87°), this model, as well as our oth-

ers, has reasonable values for the important parameters. Hence, we believe that our results describe the global qualitative properties of ACR acceleration at the termination shock, so that only minor fine-tuning is necessary if a more accurate data/theory comparison is desired.

Finally, we note that pickup ions are not absolutely necessary for producing the ACRs. The dot-dashed and dotted lines in Figure 10 show proton spectra produced for Model III when *only thermal protons* are injected at the termination shock. The effect the superthermal pickup ions have on the overall acceleration efficiency is dramatic in the case where $\eta = 5$ (without them the intensity at ACR energies drops by ~ 10 orders of magnitude), but for stronger scattering, the ACR intensities could be produced solely from thermal ions. The dotted curve shows the spectrum produced, without pickup ions, assuming $\eta = 1$, i.e. the Bohm limit. While pickup ions are clearly dominant in the production of ACRs (charge states unambiguously show this), it is important to note that some acceleration of thermal ions does occur and the relative importance will depend on the strength of scattering.

4. DISCUSSION

4.1. *Issues Concerning Ion Injection*

Various proposals for a pre-injection acceleration phase at highly oblique shocks have been put forward in the literature, a number of which were mentioned in the Introduction. While these hypotheses may have stemmed from many reports of "injection problems" for ACRs, and may indeed arise at the termination shock, the results of this paper have shown that the solar wind termination shock can easily inject and accelerate pickup ions to anomalous cosmic ray energies and intensities if standard diffusive shock acceleration operates. Hence, we find that *no pre-injection stage is necessary*; the only requirement for injection and acceleration of pickup ions consistent with ACR observations is that strong enough magnetic turbulence be present near the termination shock (i.e. $\lambda_\parallel \sim 10\,r_g$, implying $\kappa_\perp/\kappa_\parallel \sim 0.01$) to produce cross-field diffusion. Self-generated turbulence of this strength or greater is seen or inferred near a host of other astrophysical shocks, including highly oblique interplanetary shocks with parameters not too different from what is expected at the termination shock (e.g. see the recent analysis of *in situ* Ulysses observations by Baring et al. 1997).

In this paper we have also shown that while the injection efficiency depends fairly strongly on the shock obliquity and η, the character of the injection does not and varies smoothly over a range of parameters. Furthermore, small changes in the shape of the pickup ion distribution produce no noticeable effect on the injection and acceleration efficiencies. Our results seem consistent with the fact that all directly observed collisionless shocks, with the sole exception of the highly oblique Earth bow shock, accelerate thermal ions directly and diffusively with reasonable efficiencies. At the quasi-perpendicular bow shock, the unique geometry (where the solar wind constantly sweeps the magnetic field and particles past the relatively tiny tangent point) prevents self-generated turbulence from forming in the quasi-perpendicular precursor and readily explains why particle acceleration there is restricted to reflected beams (e.g. Ipavich 1988). In highly oblique inter-

planetary shocks on the other hand, the geometry is quite different (and similar to that expected at the termination shock), with injection being effected on quite small spatial scales and diffusive particle injection and acceleration readily occurs even for thermal solar wind particles (e.g. Baring et al. 1997).

Particle injection at oblique shocks is, in fact, more difficult than at parallel ones (e.g. Jokipii 1987) because downstream shock heated particles have a harder time returning to the shock; they move largely along the oblique field lines if scattering is weak. For injection to be efficient without energetic seed particles, particularly at high Mach numbers, the scattering must be reasonably strong and cross-field diffusion must take place for injection to occur (see Ellison, Baring, & Jones 1996 for a general discussion of injection efficiency in oblique shocks). Background magnetic turbulence in the undisturbed solar wind appears not to be strong enough to provide this cross-field diffusion, and it is not obvious that the termination shock can generate enough local magnetic turbulence to produce it. This has led to computer plasma simulations analogous to the Quest (1988) work on parallel shocks, and these studies thus far have suggested that pickup ions *cannot* be injected directly at the quasi-perpendicular termination shock. For instance, Kucharek & Scholer (1995) obtained results with a one-dimensional hybrid simulation that showed *no injection* of pickup ions for $\Theta_{Bn} \gtrsim 60°$. Similar results were obtained by Liewer, Rath, & Goldstein 1995. Unfortunately, because of the extreme computing requirements of three-dimensional simulations, the self-consistent hybrid simulations have so far been done mainly in restricted dimensionality. Jokipii, Kóta, & Giacalone (1993) showed (see also the more detailed derivation of Jones, Jokipii, & Baring 1998, and also Giacalone & Jokipii 1994 and Giacalone 1994 for simulation work) that the presence of an ignorable coordinate results in an artificial suppression of cross-field transport. Thus, the essential physics needed for injection has not been modeled correctly in the self-consistent one- and two-dimension hybrid simulations so far applied to the termination shock. This may also have led to the assertion that a pre-injection stage is necessary when, in fact, full three-dimensional hybrid simulations (run long enough, with enough particles, in a large enough simulation box to allow for the development of mature turbulence and particle acceleration) are required to definitively answer this question.

We note that when ad hoc scattering, which allows cross-field scattering, is added to a one-dimensional hybrid simulation (Giacalone, Jokipii, & Kóta 1994), particle injection does take place at perpendicular shocks. These simulations are still severely restricted in dynamic range and cannot produce energies typical of ACRs, but as far as we can tell, they do see the beginnings of injection and seem consistent with our results as far as a comparison can be made. *It must be emphasized that the only injection problem that exists for quasi-perpendicular shocks is whether or not magnetic turbulence of the required wavelengths to interact with shock heated ions is strong enough to produce cross-field diffusion.* If it is, we know of nothing in the Fermi mechanism that will prevent injection and acceleration.

4.2. Comparison with Other Models of ACR Production

A number of models of ACR acceleration have been presented which solve numerically the so-called Parker transport equation (e.g. Parker 1965) or similar kinetic equations which require near-isotropic distributions. Jokipii and co-workers (e.g. Jokipii & Giacalone 1996) solve the full equation in two-dimensions for a spherical termination shock and follow the acceleration of superthermal particles (i.e. $\gtrsim 100$ keV/nuc) in a realistic solar wind configuration. They include the Parker spiral magnetic field, curvature and gradient drifts, adiabatic losses, charge stripping, an equatorial current sheet, and 11-year sunspot cycle magnetic field reversals. The superthermal particles are injected as test-particles and their distribution function is followed during acceleration and propagation to an observation point in the inner heliosphere. The turnover of the ACR spectra near 150 MeV/A comes naturally in this model from the potential drop between the pole and the equator and only depends on the rotation rate of the sun and the magnetic-field strength. In all of the above respects, except for treating the accelerated particles as test-particles and starting ACRs off as mildly energetic rather than at solar wind or pickup ion energies to ensure their distributions are nearly isotropic, the Jokipii model is more complete than ours and has been successful in modeling ACR spectral shapes (including multiply charged ACRs; Jokipii 1996), latitudinal gradients, and other aspects of solar modulation.

Le Roux, Potgieter, & Ptuskin (1996) (see also Le Roux & Fichtner 1997) investigate the acceleration and modulation of ACRs including the modification of the termination shock from the pressure of the ACRs as well as galactic cosmic rays. They solve the transport equation and determine the shock structure with a set of time-dependent conservation equations. While this model is quite advanced, they obtain multiple solutions (i.e. le Roux & Fichtner 1997) with quite different values for their free injection parameter. Chalov & Fahr (1996a) present a so-called three-fluid model (solar wind plasma, pickup ions, and ACRs) which also yields the shock structure under the influence of ACR acceleration. Again, as with all fluid models of shock structure, injection is treated parametrically and all results depend critically on the injection parameter.

In contrast, our approach has concentrated on the injection process and the self-consistent determination of the shock structure in the plane-shock approximation, assuming that other aspects, such as a realistic geometry and detailed propagation models, have a lesser effect on the observed ACR spectra or at least on spectra at the termination shock. Because we do not have spherical geometry which would result in adiabatic losses (to be addressed in the next phase of our work), we must artificially impose a free escape boundary to give the observed high energy cutoff, nevertheless, we feel the most important difference between our model and previous ones, is that we treat the injection process in an automatic and more or less self-consistent fashion. The efficiency of injection is determined mostly by the value of the parameter $\eta = \lambda_{\parallel}/r_g$.

To our knowledge, all previous models applied to the termination shock and based on the transport equation have required particle speeds, v, to satisfy

$$\lambda_{\parallel}/r_g \ll v/V_{sk} \qquad (19)$$

or some similar condition. That is, particles that end up as ACRs must start off with speeds $v \gg V_{sk}$. This condition *ensures* efficient injection (e.g. Jokipii 1987), and guarantees near-isotropy of the distribution functions, a byproduct that permits use of the diffusion approximation that is central to most transport equation approaches. In contrast, our Monte Carlo technique effectively finds solutions to the more fundamental Boltzmann equation, makes no fluid approximations, places no restrictions on the isotropy of the particle distribution functions, and relates the injection efficiency to more fundamental aspects of the plasma microphysics. Moreover, we find that efficient injection is secured in our simulations, even in nearly perpendicular geometry, when $\eta = \lambda_{\parallel}/r_g \lesssim v/V_{sk}$ is satisfied, a condition that renders the collision timescale $\lambda_{\parallel}/v$ comparable to or shorter than the time r_g/V_{sk} it takes a complete particle gyro-orbit to convect through the shock.

The automatic nature of injection in our model arises principally because we assign similar diffusion properties [i.e. Equation (1)] to all particles, regardless of whether they are thermal or highly energetic. While this differs from other approaches, we note that for at least some range of particle speeds, all models of the termination shock must start with an equation similar to our equation (1). Jokipii & Giacalone (1996) assume that

$$\kappa_{\parallel} = 1.5 \times 10^{22} \beta \left(\frac{R}{10^9 V} \right)^{0.5} \mathrm{cm}^2 \mathrm{s}^{-1} \qquad (20)$$

and that $\kappa_{\perp} = 0.1\kappa_{\parallel}$, where $\beta = v/c$ and $R = pc/(Qe)$ is the particle rigidity in cgs units (c is the speed of light and e is the electronic charge). If the kinetic theory result $\kappa_{\perp} = \kappa_{\parallel}/(1 + \eta^2)$ is assumed, this gives $\eta \sim 3$, i.e. extremely strong cross-field diffusion. Chalov & Fahr (1996a) assume even stronger scattering (i.e. $\kappa_{\perp} \simeq \kappa_{\parallel}$ for MeV particles), while le Roux, Potgieter, & Ptuskin (1996) assume

$$\kappa_{\parallel} = 3.3 \times 10^{22} \left(\frac{B_1}{10^{-6} G} \right)^{-1} \eta \beta \left(\frac{R}{10^9 V} \right) \mathrm{cm}^2 \mathrm{s}^{-1}, \qquad (21)$$

for $R > 0.4$ GV and set $R = 0.4$ GV at lower rigidities. Le Roux et al. also add an extra parameter, b, introduced through $\kappa_{\perp} = b \kappa_{\parallel}/(1+\eta^2)$ to allow the simultaneous fit to 1987 observations of ACR and galactic cosmic ray spectra and use $\eta = 56$ and $b = 47$, giving $\kappa_{\perp} = 0.015\kappa_{\parallel}$. This signals a departure from kinetic theory that presumably might arise with substantial field line wandering. We emphasize that in our model, no such added parameters are necessary to reproduce the ACR hydrogen flux level in the Voyager data.

Through equation (1), our model possesses a parallel diffusion coefficient that is strongly rigidity-dependent for all momenta and is, in fact, identical to equation (21), including the numerical coefficient. Note that contrary to Le Roux et al., we assume equation (21) holds at *all* rigidities. In any case, minor differences in the energy dependence and normalization of $\kappa_{\parallel}$ are unlikely to be important. What we do believe is important is that, by including the injection and shock modification coherently with the acceleration to the highest ACR energies, we can determine the *absolute acceleration efficiency* as a function of η and other parameters. This allows us to estimate the η

needed to produce observed ACR intensities and to relate this microphysical parameter to macrophysical ones (e.g. Θ_{Bn} and Mach number).

Our fundamental result is that standard diffusive shock acceleration allows for the injection and acceleration of pickup ions to ACRs energies with the observed spectral shapes and absolute intensities if scattering of the strength that is typically assumed in current models is applied to all particles. There is no threshold energy or speed required for shock acceleration to occur. The injection process is a continuous one with the efficiency being a smoothly increasing function of the scattering intensity and does not depend critically on any of the parameters we use. We see no need to invoke complications such as field line wandering even though it's obvious that if large scale motions of the magnetic field are present, they may produce modest changes in the efficiency and modulation (e.g. le Roux, Potgieter, & Ptuskin 1996). It also seems likely that whatever field line wandering is present is not self-generated but comes from an independent background. If the termination shock is producing self-generated turbulence of the intensities assumed by current models, this turbulence should be much more intense than any background turbulence.

We also showed from efficiency considerations that less oblique regions of the termination shock are less likely to contribute a significant fraction of the ACRs. Unless much more complicated models are imagined, the only way to obtain intensities consistent with the observed ACR intensities and estimates of pickup ion densities at portions of the termination shock that have Θ_{Bn} significantly smaller than $90°$, is by reducing the scattering efficiency, i.e. by increasing η. Increasing η causes time and length scales to increase and these can become inconsistent with the termination shock size and charge-stripping rates. This seems to conflict with the analytic results of Chalov & Fahr (1996b) and those stemming from one- or two-dimensional hybrid simulations, which conclude that only regions with moderate obliquity ($\Theta_{Bn} \lesssim 75°$ for Chalov & Fahr and $\Theta_{Bn} \lesssim 60°$ for hybrid results) can be producing ACRs.

Finally, while we obtain He^+/H^+ and O^+/H^+ ratios which are somewhat smaller than reported by Cummings & Stone (1996), we definitely see an A/Q enhancement effect during acceleration, as illustrated in Figure 7. We note that the lower Mach number example tends to produce larger A/Q enhancements due to a complex interplay between shock parameters such as η, Θ_{Bn1}, and Mach number, which we adjust to obtain the same ACR H^+ flux. For low Mach number shocks, with lower compression ratios, η must be smaller (i.e. the scattering must be stronger) to allow increased injection to end up with the observed ACR fluxes. For our Model III, we obtain enhancements for He^+ and O^+ over H^+ of ~ 4 and 6, respectively, which is about a factor of 4 less than that inferred by Cummings & Stone (1996). It is not clear why our enhancements are less, but it may suggest that there are effects not included in our model which will increase the acceleration efficiency of heavy ions relative to protons. However, adding a cross-shock potential (an obvious extension of our model) might well lead to enhanced proton acceleration relative to heavier ions, worsening the discrepancy. For now, we leave this as an important unsolved problem.

5. CONCLUSIONS

In this paper, we have shown that diffusive shock acceleration operating at the termination shock can account for observed ACR proton fluxes by directly accelerating pickup ions from solar wind speeds to $\sim$ 150 MeV. The only requirements for direct injection is that local magnetic turbulence exists (presumably self-generated) such that $\kappa_\perp/\kappa_\parallel \gtrsim 0.01$ and that $\lambda_\parallel$, for pickup ions injected at the shock, is a small fraction of an AU. These criteria are not difficult to satisfy in heliospheric environments, so we suggest that previous work claiming that a pre-acceleration stage is *required* for diffusive shock acceleration to explain ACR production at the termination shock was based on incomplete modeling of the acceleration process. We believe this is the first calculation of the *absolute* intensities of ACRs using standard solar wind quantities and basic microphysical parameters. We find that the acceleration process at the termination shock is, as far as limited observations allow us to determine, identical in all important respects to diffusive particle acceleration observed at inner heliospheric systems such as the Earth bow shock and travelling interplanetary shocks.

REFERENCES

Achterberg, A., Blandford, R. D. & Reynolds, S. P. 1994, A&A 281, 220.

Adams, J. H. & Leising, M. D. 1991, in Proc. 22nd ICRC (Dublin), 3, 304.

Axford, W. I. 1965, Planet. Sp. Sci. 13, 1301.

Baring, M. G., Ellison, D. C., & Jones, F. C. 1994, ApJS 90, 547.

Baring, M. G., Ellison, D. C., & Jones, F. C. 1995, Adv. Space Res. 15(8/9), 397.

Baring, M. G., Ogilvie, K. W., Ellison, D. C., & Forsyth, R. J. 1997, ApJ 476, 889.

Bieber, J. W., Matthaeus, W. H., Smith, C. W., Wanner, W., Kallenrode, M.-B., & Wibberenz, G. 1994, ApJ 420, 294.

Bogdan, T. J., Lee, M. A., & Schneider, P. 1991, J. Geophys. Res. 96, 161.

Chalov, S. V., & Fahr, H. J. 1996a, A&A 311, 317.

Chalov, S. V., & Fahr, H. J. 1996b, Sol. Phys. 168, 389.

Christian, E. R., Cummings, A. C., & Stone, E. C. 1995, ApJ 446, L105.

Cummings, A. C., & Stone, E. C. 1996, Space Sci. Rev. 78, 117.

Drury, L. O'C. 1983, Rep. Prog. Phys. 46, 973.

Eichler, D. 1979, ApJ 229, 419.

Ellison, D. C., Drury, L. O'C., & Meyer, J. P. 1997, ApJ 487, 197.

Ellison, D. C., Baring, M. G., & Jones, F. C. 1995, ApJ 453, 873.

Ellison, D. C., Baring, M. G., & Jones, F. C. 1996, ApJ 473, 1029.

Ellison, D. C., Jones, F. C., & Eichler, D. 1981, Journal of Geophysics, 50, 110.

Ellison, D. C., Möbius, E., & Paschmann, G. 1990, ApJ 352, 376.

Fichtner, H., le Roux, J. A., Mall, U., & Rucinski, D. 1996, A&A 314, 650.

Fisk, L. A. 1976, J. Geophys. Res. 81, 4633.

Fisk, L. A. 1996, Space Sci. Rev. 78, 129.

Fisk, L. A., Kozlovsky, B., & Ramaty, R. 1974, ApJ 190, L35.

Fisk, L. A., Schwadron, N. A., & Gloeckler, G. 1997, Geophys. Res. Lett. 24, 93.

Forman, M. A., Jokipii, J. R. & Owens, A. J. 1974, ApJ 192, 535.

Geiss, J., Gloeckler, G., Mall, U., von Steiger, R., Galvin, A. B., & Ogilvie, K. W. 1994, A&A 282, 924.

Giacalone, J. 1994, Geophys. Res. Lett. 21, 2441.

Giacalone, J., Burgess, D., Schwartz, S. J., & Ellison, D. C. 1993, ApJ 402, 550.

Giacalone, J., & Jokipii, J. R. 1994, ApJ 430, L137.

Giacalone, J., Jokipii, J. R., & Kóta, J. 1994, J. Geophys. Res. 99, 19,351.

Gloeckler, G. 1996, Space Sci. Rev. 78, 335.

Gloeckler, G., Fisk, L. A., & Geiss, J. 1997, Nature 386, 374.

Gloeckler, G., Geiss, J., Fisk, L. A., Galvin, A. B., Ipavich, F. M., Ogilvie, K. W., von Steiger, R., & Wilken, B. 1993, Science, 261, 70.

Gloeckler, G., Geiss, J., Roelof, E. C., Fisk, L. A., Ipavich, F. M., Ogilvie, K. W., Lanzerotti, L. J., von Steiger, R., & Wilken, B. 1994, J. Geophys. Res. 99, 17,637.

Gloeckler, G., Schwadron, N. A., Fisk, L. A., & Geiss, J. 1995, Geophys. Res. Lett. 22, 2665.

Ipavich, F. M., Gloeckler, G., Hamilton, D. C., Kistler, L. M., & Gosling, J. T. 1988, Geophys. Res. Lett. 15, 1153.

Isenberg, P. A. 1986, J. Geophys. Res. 91, 9965.

Isenberg, P. A. 1997, Geophys. Res. Lett. 24, 623.

Jokipii, J. R. 1987, ApJ 312, 170.

Jokipii, J. R. 1992, ApJ 393, L41.

Jokipii, J. R. 1996, ApJ 466, L47.

Jokipii, J. R., & Giacalone, J. 1996, Space Sci. Rev. 78, 137.

Jokipii, J. R., Kóta, J., & Giacalone, J. 1993, Geophys. Res. Lett. 20, 1759.

Jones, F. C. 1990, ApJ 361, 162.

Jones, F. C., & Ellison, D. C. 1991, Space Sci. Rev. 58, 259.

Jones, F. C., Jokipii, J. R., & Baring, M. G. 1998, ApJ in press.

Kucharek, H., & Scholer, M. 1995, J. Geophys. Res. 100, 1745.

Lee, M. A. 1982, J. Geophys. Res. 87, 5063.

Lee, M. A. 1983, J. Geophys. Res. 88, 6109.

Lee, M. A., Shapiro, V. D., & Sagdeev, R. Z. 1996, J. Geophys. Res. 101, 4777.

Le Roux, J. A., & Fichtner, H. 1997, ApJ 477, L115.

Le Roux, J. A., Potgieter, M. S., & Ptuskin, V. S. 1996, J. Geophys. Res. 101, 4791.

Liewer, P. C., Rath, S., & Goldstein, B. E. 1995, J. Geophys. Res. 100, 19,809.

Mewaldt, R. A., Selesnick, R. S., Cummings, J. R., Stone, E. C., & von Rosenvinge, T. T. 1996, ApJ 466, L43.

Möbius, E., Rucinski, D., Lee, M. A., & Isenberg, P. A. 1998, J. Geophys. Res. 103, 257.

Moussas, X., Quenby, J. J., Theodossiou-Ekaterinidi, Z., Valdes-Galicia, J. F., Drillia, A. G., Roulias, D. & Smith, E. J. 1992, Sol. Phys. 140, 161.

Ostrowski, M. 1988, MNRAS 233, 257.

Palmer, I. D. 1982, Rev. Geophys. & Sp. Phys. 20, 335.

Parker, E. N. 1958, ApJ 128, 664.

Parker, E. N. 1965, Planet. Sp. Sci. 13, 9.

Pesses, M. E., Jokipii, J. R., & Eichler, D. 1981, ApJ 246, L85.

Phillips, J. L., et al., 1995, Space Sci. Rev. 72, 109.

Rucinski, D., Fahr, H. J., & Grzedzielski, S. 1993, Planet. Sp. Sci. 41, 773.

Rucinski, D., et al. 1996, Space Sci. Rev. 78, 73.

Quest, K. B. 1988, J. Geophys. Res. 93, 9649.

Schwadron, N. A., Fisk, L. A., & Gloeckler, G. 1996, Geophys. Res. Lett. 23, 2871.

Stone, E. C., Cummings, A. C., & Webber, W. R. 1996, J. Geophys. Res. 101, 11,017.

Vasyliunas, V. M., & Siscoe, G. L. 1976, J. Geophys. Res. 81, 1247.

Zank, G. P., Pauls, H. L., Cairns, I. H., & Webb, G. N. 1996, J. Geophys. Res. 101, 457.